# Elastic Registration based on Matrix-Valued Spline Functions and Direct Integration of Landmarks and Intensities

Stefan Wörz, Andreas Biesdorf, and Karl Rohr

University of Heidelberg, BIOQUANT, IPMB, and DKFZ Heidelberg, Germany
Dept. Bioinformatics and Functional Genomics, Biomedical Computer Vision Group,
Im Neuenheimer Feld 267, 69120 Heidelberg, Germany
E-mail: s.woerz@dkfz.de

## ABSTRACT

We introduce a new approach for spline-based elastic registration using both point landmarks and intensity information. With this approach, both types of information and a regularization based on the Navier equation are directly integrated in a single energy minimizing functional. For this functional, we have derived an analytic solution, which is based on matrix-valued non-radial basis functions. Our approach can cope with monomodal and multimodal images. For the latter case, we have integrated a computationally efficient analytic similarity measure. We have successfully applied our approach to synthetic images, phantom images, and MR images of the human brain.

**Keywords:** Hybrid elastic registration, Landmarks and intensities, Mutual information, Analytic solution

## 1. INTRODUCTION

Monomodal and multimodal registration of 2D and 3D images is an important task in medical image analysis, where generally nonrigid or elastic schemes are required. Often, *spline-based* approaches have been used for elastic registration, which can be subdivided into schemes based on a uniform grid of control points (e.g., using B-splines,[1–3]), and schemes based on a nonuniform grid of control points (e.g.,[4–9]). The latter type of approaches generally requires a smaller number of control points (landmarks). Examples of such approaches are based on thin-plate splines (TPS, e.g.,[5–7]), elastic body splines (EBS, e.g.,[4]), and Gaussian elastic body splines (GEBS, e.g.,[8,9]). TPS are based on the bending energy of a thin plate and thus represent a relatively coarse deformation model for biological tissues. In contrast, EBS and GEBS are derived from the Navier equation, which describes the deformation of elastic tissues (bodies). GEBS in comparison to EBS have the advantage that more realistic forces are used. Registration approaches are typically based on either landmarks or intensity information. Main advantages of *landmark-based* approaches are computational efficiency and the ability to cope with large geometric differences as well as the relatively easy and intuitive incorporation of user-interaction. In comparison, main advantages of *intensity-based* approaches are that all image information is exploited and that no segmentation is necessary. For the latter type of approaches, it is important to distinguish between monomodal and multimodal registration problems. For *monomodal* registration, often the sum-of-squared intensity differences (SSD) is used. Registration of images of different modalities, however, requires *multimodal* similarity measures such as mutual information (MI). In general, measures for MI are computationally expensive because they require the estimation of probability density functions based on joint histograms (e.g.,[1]). In recent years, *hybrid* approaches that combine landmark- and intensity-based methods have gained increased attention (e.g.,[2,3,6,10,11]). However, so far only few *spline-based* hybrid registration approaches exist. Typically, the intensity information is only used to determine optimal landmark positions or to establish landmark correspondences (e.g.,[3]), i.e., the landmark and intensity information is not directly combined. In addition, often a physical deformation model is not used (e.g.,[2,3]).

In this contribution, we introduce a new approach for spline-based elastic registration using both point landmarks and intensity information. Compared to previous *spline-based* hybrid registration approaches, we directly integrate the landmark and intensity information in a single energy functional as well as include a regularization using matrix-valued physically-based basis functions. Note that in contrast to,[12,13] we directly incorporate the landmark correspondences without requiring an additional deformation field for the landmarks.

Medical Imaging 2012: Image Processing, edited by David R. Haynor, Sébastien Ourselin,
Proc. of SPIE Vol. 8314, 83141B · © 2012 SPIE · CCC code: 0277-786X/12/$18 · doi: 10.1117/12.911414

An advantage is that the intensity and landmark information can be weighted w.r.t. each other more directly and thus the weighting is easier to control. The approach is formulated as an energy functional, for which we show that an analytic solution can be derived via the convolution theorem. In addition to using the SSD for the monomodal case, we incorporate a multimodal intensity similarity measure. This similarity measure is based on a local analytic formulation for MI, which is computationally efficient since it does *not* require the estimation of probability density functions and joint histograms.

## 2. INTERPOLATING AND APPROXIMATING GEBS

In our approach, we use Gaussian elastic body splines (GEBS) as underlying deformation model. Below, we briefly review the interpolating and approximating landmark-based approaches.

### 2.1 Interpolating GEBS

*Interpolating* GEBS are based on the Navier equation of linear elasticity (e.g.,[14])

$$\mu \Delta \mathbf{u} + (\lambda + \mu) \nabla (\operatorname{div} \mathbf{u}) + \mathbf{f} = \mathbf{0} \tag{1}$$

with the displacement vector field $\mathbf{u}$, body forces $\mathbf{f}$, and the Lamé constants $\mu, \lambda > 0$ describing material properties. Given Gaussian forces $\mathbf{f}_\sigma(\mathbf{x}) = \mathbf{c}\, f_\sigma(r) = \mathbf{c}\, (\sqrt{2\pi}\sigma)^{-3} \exp(-\frac{r^2}{2\sigma^2})$ with $\mathbf{x} = (x, y, z)^T$, $r = \sqrt{x^2 + y^2 + z^2}$, and the standard deviation $\sigma$, an analytic solution of the Navier equation can be derived, which is based on a matrix-valued basis function $\mathbf{G}_\sigma$ (a $3 \times 3$ matrix).[8] Using the interpolation condition $\mathbf{q}_i = \mathbf{u}(\mathbf{p}_i)$, where $\mathbf{p}_i$ and $\mathbf{q}_i$ $(i = 1, \ldots, n)$ denote the $n$ landmark positions of the source and target image, respectively, the transformation is given by $\mathbf{u}(\mathbf{x}) = \mathbf{x} + \sum_{i=1}^{n} \mathbf{G}_\sigma(\mathbf{x} - \mathbf{p}_i)\, \mathbf{c}_i$. The coefficients $\mathbf{c}_i$ represent the strength and direction of the Gaussian forces and are computed using a linear system of equations (LSE) such that the interpolation condition is fulfilled for all landmarks.

### 2.2 Approximating GEBS

In comparison, *approximating* GEBS are based on the condition $\mathbf{q}_i \approx \mathbf{u}(\mathbf{p}_i)$ and incorporate covariance matrices $\mathbf{\Sigma}_i$ defining anisotropic landmark localization uncertainties. The energy-minimizing functional consists of an elastic term $J_{Elastic}$ representing the elastic energy according to the Navier equation as well as a quadratic data term $J_{Data,L}$ which incorporates the landmark errors. The corresponding Lagrange function $L_{Data,L}$ with $J_{Data,L} = \int L_{Data,L}\, d\mathbf{x}$ is given by

$$L_{Data,L} = (n\lambda_A)^{-1} \sum\nolimits_{i=1}^{n} f_\sigma(\mathbf{x} - \mathbf{p}_i)\, (\mathbf{q}_i - \mathbf{u}(\mathbf{x}))^T\, \mathbf{\Sigma}_i^{-1}\, (\mathbf{q}_i - \mathbf{u}(\mathbf{x})) \tag{2}$$

where $\lambda_A > 0$ denotes the regularization parameter. The solution to the corresponding PDE can be derived analytically and is based on the same basis function $\mathbf{G}_\sigma$ as in the case of interpolation.[9]

## 3. HYBRID ELASTIC REGISTRATION USING SPLINE FUNCTIONS

In the following, we introduce a *hybrid* approach for the registration of monomodal and multimodal images, where both landmark and intensity information is incorporated and GEBS are used as deformation model. To compute the deformation field $\mathbf{u}$ for registering a source image $g_1$ with a target image $g_2$, we propose the functional

$$J_{Hybrid}(\mathbf{u}) = \lambda_E\, J_{Elastic}(\mathbf{u}) + J_{Data,I}\left(g_1, g_2, \mathbf{u}^I\right) + \lambda_I J_I\left(\mathbf{u}, \mathbf{u}^I\right) + J_{Data,L}((\mathbf{p}_i, \mathbf{q}_i), \mathbf{u})\,. \tag{3}$$

The *functional* has been formulated in a way such that the minimization w.r.t. the searched deformation field $\mathbf{u}$ can be obtained in analytic form. The functional also comprises a deformation field $\mathbf{u}^I$ that is computed based on the *intensity* information. The first term $J_{Elastic}$ represents the *regularization* of $\mathbf{u}$, and is given by the elastic energy according to the Navier equation. In addition, the functional comprises terms for the intensity information and the landmark information, which are described below.

### 3.1 Intensity Information

The second term $J_{Data,I}$ of (3) represents an intensity similarity measure between the deformed source and target image with deformation $\mathbf{u}^I$. The third term $J_I$ couples $\mathbf{u}^I$ with $\mathbf{u}$ using a weighted Euclidean distance. Based on the considered application, different intensity similarity measures can be used. For monomodal images we use the *sum-of-squared intensity differences* (SSD)

$$J_{Data,I,SSD}\big(g_1, g_2, \mathbf{u}^I\big) = \int \big(g_1\big(\mathbf{x} + \mathbf{u}^I(\mathbf{x})\big) - g_2(\mathbf{x})\big)^2 \, d\mathbf{x}. \tag{4}$$

For multimodal images we use *mutual information* (MI). The idea is to evaluate the intensity information *locally* based on an analytic measure for MI.[15] The measure is computationally efficient since it does *not* require the estimation of probability density functions and joint histograms. The measure was theoretically derived based on the Taylor approximation of the intensities and considering them as samples of a random distribution. A similar measure was previously used in[16,17] while the relation to MI was not known. In contrast to,[15–17] where the measure is optimized *globally*, in our approach we perform a *local* optimization. Based on a local image approximation, the mutual information at a single voxel $\mathbf{x}$ can be formulated as

$$MI(g_1(\mathbf{x}), g_2(\mathbf{x})) = c - \log_2(|\sin\theta|) \tag{5}$$

where $\theta$ denotes the angle between the gradients $\nabla g_1$ and $\nabla g_2$ of the source and target image, respectively. $c$ is a constant which is not relevant for minimization. The corresponding functional of the local MI measure can be formulated as

$$J_{Data,I,MI}\big(g_1, g_2, \mathbf{u}^I\big) = \int MI\big(g_1\big(\mathbf{x} + \mathbf{u}^I\big), g_2(\mathbf{x})\big) \; d\mathbf{x}. \tag{6}$$

### 3.2 Landmark Information

The fourth term $J_{Data,L}$ of (3) describes the *landmark* information based on $n$ landmark correspondences $(\mathbf{p}_i, \mathbf{q}_i)$. To incorporate anisotropic localization uncertainties we employ approximating GEBS (see Sect. 2.2 above). The idea is to use the approximating functional $J_{Data,L} = \int L_{Data,L}\, d\mathbf{x}$ defined by the Lagrange function $L_{Data,L}$ in (2). Therefore, we here *directly* incorporate the landmark correspondences $(\mathbf{p}_i, \mathbf{q}_i)$. In contrast, in the approach in[12,13] a third deformation field $\mathbf{u}^L$ is required for the landmark information analogously to the intensity information using $\mathbf{u}^I$. An advantage of the previous approach is that the mathematical derivation and implementation of the minimization scheme is easier. However, a main drawback is that the additional deformation field $\mathbf{u}^L$ has a strong global influence since it is computed for the whole image (i.e., also for regions without landmarks) which results in a compromise between $\mathbf{u}^I$ and $\mathbf{u}^L$. In contrast, with the new approach the landmark information is directly exploited in the vicinity of the landmarks. Thus, the intensity and landmark information can be weighted more directly w.r.t. each other and the weighting is easier to control.

### 3.3 Minimization Strategy

An efficient way of minimizing $J_{Hybrid}$ in (3) is to minimize it alternatingly w.r.t. $\mathbf{u}^I$ and $\mathbf{u}$ until convergence of $\mathbf{u}$ is achieved. To initialize $\mathbf{u}$, we use a deformation field computed from the landmark correspondences using approximating GEBS. For the minimization w.r.t. $\mathbf{u}^I$, the following functional is relevant:

$$J_{Data,I}\big(g_1, g_2, \mathbf{u}^I\big) + \lambda_I J_I\big(\mathbf{u}, \mathbf{u}^I\big) \to \min. \tag{7}$$

For the intensity similarity measures $J_{Data,I}$, i.e., sum-of-squared intensity differences (SSD) and mutual information (MI), we use Levenberg/Marquardt and gradient descent minimization, respectively.

For the minimization w.r.t. $\mathbf{u}$, the following functional has to be considered

$$\lambda_E \, J_{Elastic}(\mathbf{u}) + \lambda_I J_I\big(\mathbf{u}, \mathbf{u}^I\big) + J_{Data,L}((\mathbf{p}_i, \mathbf{q}_i), \mathbf{u}) \to \min. \tag{8}$$

The corresponding PDE can be derived as (using $\epsilon_I = 2\lambda_I/\lambda_E$)

$$\mathbf{0} = \mu\Delta\mathbf{u} + (\lambda + \mu)\,\nabla\,(\operatorname{div}\mathbf{u}) + \epsilon_I \int f_{\sigma_I}(\mathbf{x} - \boldsymbol{\xi})\,\big(\mathbf{u}^I(\boldsymbol{\xi}) - \mathbf{u}(\mathbf{x})\big)\, d\boldsymbol{\xi} + 2\lambda_A \sum\nolimits_{i=1}^{n} f_\sigma(\mathbf{x} - \mathbf{p}_i)\,\boldsymbol{\Sigma}_i^{-1}\,(\mathbf{q}_i - \mathbf{u}(\mathbf{x}))\,. \tag{9}$$

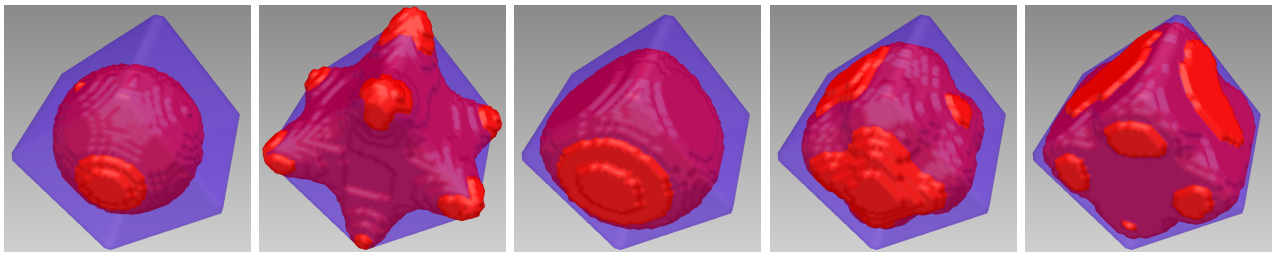

Unregistered Landmarks Intensities Previous hybrid New hybrid

Figure 1. Multimodal registration of 3D synthetic images of a sphere with a cube.

Interestingly, (9) can be solved analytically by employing the convolution theorem and the Fourier transform. An explicit solution using matrix-vector convolutions as well as the intensity-based deformation field $\mathbf{u}^I$ and the matrix-valued GEBS basis function $\mathbf{G}_\sigma$ is given by

$$\mathbf{u}(\mathbf{x}) = \mathbf{x} + \mathbf{\Phi}_I(\mathbf{x}) * \big(\mathbf{u}^I(\mathbf{x}) - \mathbf{x}\big) + \mathbf{\Phi}_L(\mathbf{x}) * \sum\nolimits_{i=1}^{n} \mathbf{G}_\sigma(\mathbf{x} - \mathbf{p}_i)\ \mathbf{c}_i \tag{10}$$

where "$*$" denotes the convolution. The matrix-valued functions $\mathbf{\Phi}_I$ and $\mathbf{\Phi}_L$ are defined by matrix-matrix convolutions (using the Dirac delta function $\delta$ and the identity matrix $\mathbf{I}$)

$$\mathbf{\Phi}_I(\mathbf{x}) = \mathbf{G}_{\sigma_I}(\mathbf{x}) * \mathbf{\Omega}_I(\mathbf{x}) \quad \text{and} \quad \mathbf{\Phi}_L(\mathbf{x}) = \delta(\mathbf{x})\,\mathbf{I} - \mathbf{G}_{\sigma_I}(\mathbf{x}) * \mathbf{\Omega}_L(\mathbf{x}) \tag{11}$$

with matrix-valued functions $\mathbf{\Omega}_I$ and $\mathbf{\Omega}_L$, which are defined in the Fourier domain. Since here we directly incorporate the landmarks in $J_{Hybrid}$, the analytic solution (10), (11) is very different and more complex compared to the solution in[12,13] where a third (auxiliary) deformation field for the landmarks is required. Note that a special case of the new hybrid scheme is obtained by omitting the landmark information $J_{Data,L}$ from (3) and in subsequent equations, which results in a pure intensity-based elastic registration scheme.

## 4. RESULTS

We have applied our approach to 3D synthetic and 3D phantom images, and 2D MR images of the human brain.

### 4.1 3D Synthetic Multimodal Images

We have applied the approach to different 3D synthetic images. Fig. 1 (left), for example, shows the case of a sphere (source image) and a cube (target image) as an overlay image. Note that the images have inverted contrast to simulate a multimodal registration problem. Thus, a registration scheme using SSD would fail. Eight landmarks were defined at the corners of the cube, and the registration is computed based on mutual information. The other images in Fig. 1 show the results for landmark-based and intensity-based registration as well as for hybrid registration using a previous approach[12,13] and the new approach. It turns out that for landmark-based registration only the corners of the cube are aligned. Using the intensity-based approach, the faces of the sphere are aligned, but not the corners. With the previous approach, the result is improved compared to the landmark- and intensity-based approaches, however, the corners are not well aligned. The best result is obtained using the new approach, since both the faces and the corners are much better aligned.

To quantify the registration results, we have computed the volume and overlap of the registered sphere with the cube for all considered approaches. For the landmark-based, the intensity-based, and the previous approach, the volume of the deformed sphere is improved to about 83% of the volume of the cube with an overlap of about 77%. In comparison, using the new approach the result is significantly better, i.e., the volume is improved to about 100% and the overlap is 95.7%.

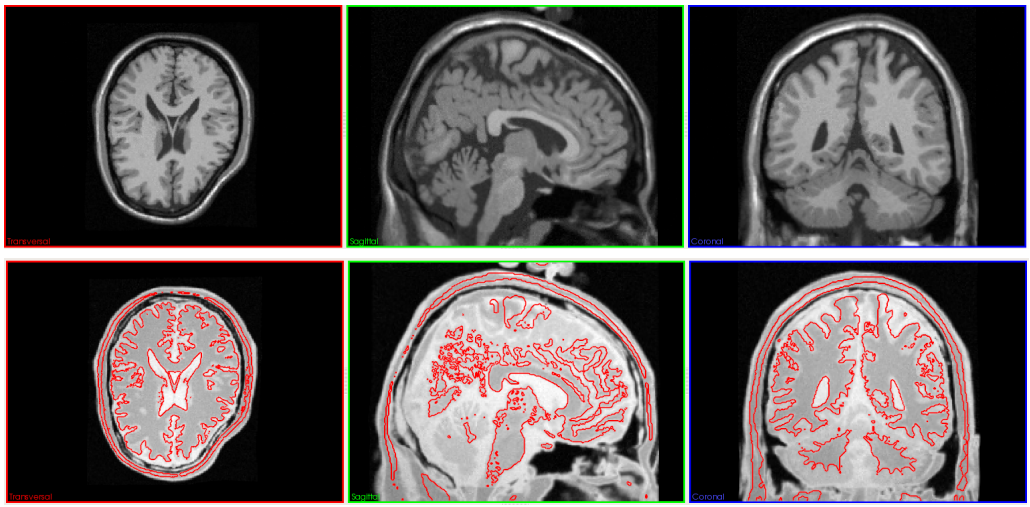

Figure 2. 3D registration of a PD image with a MRI-T1 image using mutual information: Target image (MRI-T1) with known deformation (top) as well as an overlay (bottom) of the registered source image with computed edges of the target image (red) in three orthogonal sections.

### 4.2 3D MR Phantom Images – Ground Truth Deformation

To further evaluate the registration accuracy, we have used multimodal phantom images (MRI-T1, MRI-T2, and proton density (PD)) from the BrainWeb database .[18] In this experiment, we have generated different ground truth deformation fields $\mathbf{u}_{orig}$ using Wendland splines.[19] For example, Fig. 2 (top) shows three orthogonal sections of a T1 weighted 3D MRI data set with significant deformations (target image). As source images, we have used the undeformed MRI-T1 image as well as a MRI-T2 image and a PD image. After registration, we compared the computed deformation $\mathbf{u}$ with the original deformation $\mathbf{u}_{orig}$ and quantified the registration accuracy by the mean geometric error $\overline{e}_{geom} = \overline{\|\mathbf{u}_{orig} - \mathbf{u}\|}$. For the PD image, Fig. 2 (bottom) shows an overlay of the registered source image with computed edges of the target image (red) using mutual information. It can be seen that the image has been well registered. The mean geometric error of the unregistered case is $\overline{e}_{geom} = 3.50$ voxels. After registration, the error is reduced to $\overline{e}_{geom} = 1.78$, $\overline{e}_{geom} = 2.04$, and $\overline{e}_{geom} = 2.05$ voxels for the modalities MRI-T1, MRI-T2, and PD, respectively. Thus, in all three cases, the geometric error was reduced by more than 40%.

### 4.3 2D MR Images – Tumor Resection

In this application, the task is to register pre- and postsurgical MR images of the human brain. Fig. 3 shows 2D MR images of a patient before (source image, left) and after (target image, right) the resection of a tumor. Landmarks have been placed manually along the contours of the tumor and the resection area (indicated by crosses). Furthermore, in Fig. 4 a region-of-interest of the registration results are shown as (inverse) deformation grids using a landmark-based (a), an intensity-based (b), a previous hybrid[12,13] (c), and the new hybrid approach (d). Using only *landmarks* (a), the vicinity of the tumor and resection area are well registered, whereas regions without landmarks are not deformed. In contrast, using only *intensity* information (b) yields deformations in different parts of the head, however, the tumor has not been well registered. Applying the new hybrid approach the result is significantly improved compared to both approaches since the tumor and resection area are well registered, and, in addition, other parts of the head (d). For the previous hybrid approach (c), the vicinity of the tumor and resection area is not very well aligned, i.e., the information from the landmarks is only partially used.

Moreover, for the ROI we quantitatively determined how well the results of the intensity-based and hybrid approaches agree with landmark-based registration. The latter result can be assumed to be very well in this region since a relatively large number of landmarks (17) from a medical expert were used. We have computed the mean $\overline{e}_{geom}$ and maximal geometric error $e_{geom,max}$ w.r.t. the landmark-based registration result. Using only

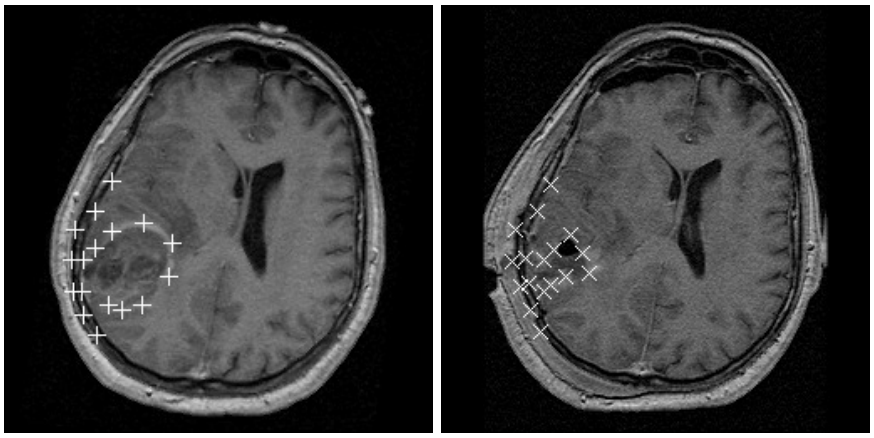

Figure 3. Pre- (left) and postsurgical 2D MR brain image (right) with labeled landmarks.

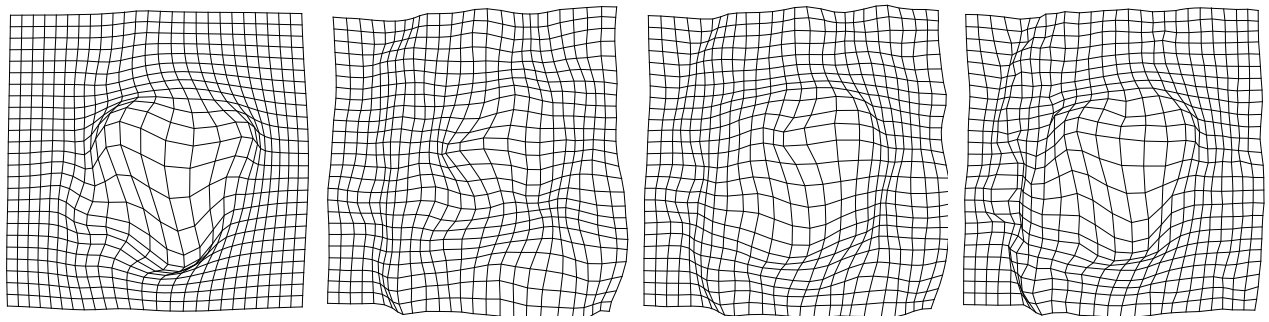

(a) (b) (c) (d)

Figure 4. ROI of (inverse) deformation grids using a landmark-based (a), an intensity-based (b), a previous hybrid[12, 13] (c), and the new hybrid approach (d).

intensity information, we obtained relatively large errors of $\overline{e}_{geom} = 4.52$ voxels and $e_{geom,max} = 19.65$ voxels. Note that in the ROI, landmark-based registration yields a maximal deformation of 21.00 voxels. Using the previous hybrid approach, the results improved to $\overline{e}_{geom} = 1.94$ voxels and $e_{geom,max} = 10.09$ voxels. However, the best result is obtained for the new hybrid approach with $\overline{e}_{geom} = 1.43$ voxels and $e_{geom,max} = 5.67$ voxels.

## 5. CONCLUSIONS

We have introduced a spline-based registration approach which directly integrates both landmark and intensity information. The approach is based on a physical deformation model represented by matrix-valued basis functions and is formulated as an energy minimizing functional. For this functional, we have derived an efficient analytic solution. Also, we have incorporated a computationally efficient multimodal intensity similarity measure, which is based on a local analytic measure for mutual information. We have demonstrated the applicability of the approach based on synthetic images, phantom images, and MR brain images. It turned out that the hybrid approach improves the registration result compared to pure landmark-based and intensity-based schemes as well as a previous hybrid scheme.


## Acknowledgment

This work has been funded by the Deutsche Forschungsgemeinschaft (DFG) within the project ELASTIR (RO 2471/2). The original MR images and the tumor outlines in Fig. 3 have kindly been provided by Prof. Dr. med. U. Spetzger and Prof. Dr. J.-M. Gilsbach, Neurosurgical Clinic, University Hospital Aachen of the RWTH.

## REFERENCES


[1] Rueckert, D., Sonoda, L., Hayes, C., Hill, D., Leach, M., and Hawkes, D., "Non-rigid Registration Using Free-Form Deformations: Application to Breast MR Images," *IEEE Trans. on Medical Imaging* **18**(8), 712–721 (1999).

[2] Kybic, J. and Unser, M., "Fast parametric elastic registration," *IEEE Trans. on Image Processing* **12**(11), 1427–1442 (2003).

[3] Stewart, C., Lee, Y.-L., and Tsai, C.-L., "An Uncertainty-Driven Hybrid of Intensity-Based and Feature-Based Registration with Application to Retinal and Lung CT Images," in [*Proc. Seventh Internat. Conf. on Medical Image Computing and Computer-Assisted Intervention (MICCAI'04)*], Barillot, C., Haynor, S., and Hellier, P., eds., *Lecture Notes in Computer Science* **3216**, 870–877, Springer Berlin Heidelberg, Rennes/Saint-Malo, France (Sept. 2004).

[4] Davis, M., Khotanzad, A., Flaming, D., and Harms, S., "A physics-based coordinate transformation for 3D image matching," *IEEE Trans. on Medical Imaging* **16**(3), 317–328 (1997).

[5] Rohr, K., Stiehl, H., Sprengel, R., Buzug, T., Weese, J., and Kuhn, M., "Landmark-Based Elastic Registration Using Approximating Thin-Plate Splines," *IEEE Trans. on Medical Imaging* **20**(6), 526–534 (2001).

[6] Johnson, H. and Christensen, G., "Consistent Landmark and Intensity-based Image Registration," *IEEE Trans. on Medical Imaging* **21**(5), 450–461 (2002).

[7] Park, H., Bland, P., Brock, K., and Meyer, C., "Adaptive registration using local information measures," *Medical Image Analysis* **8**, 465–473 (2004).

[8] Kohlrausch, J., Rohr, K., and Stiehl, H., "A New Class of Elastic Body Splines for Nonrigid Registration of Medical Images," *J. of Mathematical Imaging and Vision* **23**(3), 253–280 (2005).

[9] Wörz, S. and Rohr, K., "Physics-based elastic registration using non-radial basis functions and including landmark localization uncertainties," *Computer Vision and Image Understanding* **111**(3), 263–274 (2008).

[10] Gee, J., Haynor, D., Reivich, M., and Bajcsy, R., "Finite element approach to warping of brain images," in [*Proc. SPIE Medical Imaging 1994: Medical Imaging*], Loew, M., ed., *Proc. SPIE* **2167**, 327–337, SPIE Bellingham, WA/USA, Newport Beach, CA/USA (Feb. 1994).

[11] Hellier, P. and Barillot, C., "Coupling dense and landmark-based approaches for non rigid registration," *IEEE Trans. on Medical Imaging* **22**(2), 217–227 (2003).

[12] Wörz, S. and Rohr, K., "Hybrid Physics-Based Elastic Image Registration Using Approximating Splines," in [*Proc. SPIE Medical Imaging 2008: Image Processing*], Reinhardt, J. and Pluim, J., eds., *Proc. SPIE*, SPIE Bellingham, WA/USA, San Diego, CA/USA (Feb. 2008).

[13] Biesdorf, A., Wörz, S., Kaiser, H.-J., Stippich, C., and Rohr, K., "Hybrid Spline-Based Multimodal Registration Using Local Measures for Joint Entropy and Mutual Information," in [*Proc. Twelfth Internat. Conf. on Medical Image Computing and Computer-Assisted Intervention (MICCAI'09)*], Yang, G., Hawkes, D., Rueckert, D., Noble, A., and Taylor, C., eds., *Lecture Notes in Computer Science* **5761**, 607–615, Springer Berlin Heidelberg, London, UK (Sept. 2009).

[14] Chou, P. and Pagano, N., [*Elasticity – Tensor, Dyadic, and Engineering Approaches*], Dover Publications, Inc., New York/USA (1992).

[15] Karaçali, B., "Information theoretic deformable registration using local image information," *Internat. J. of Computer Vision* **72**(3), 219–237 (2007).

[16] Pluim, J., Maintz, J., and Viergever, M., "Image Registration by Maximization of Combined Mutual Information and Gradient Information," *IEEE Trans. on Medical Imaging* **19**(8), 809–814 (2000).

[17] Haber, E. and Modersitzki, J., "Intensity Gradient Based Registration and Fusion of Multi-modal Images," in [*Proc. Ninth Internat. Conf. on Medical Image Computing and Computer-Assisted Intervention (MICCAI'06)*], Larsen, R., Nielsen, M., and Sporring, J., eds., *Lecture Notes in Computer Science* **4191**, 726–733, Springer Berlin Heidelberg, Copenhagen, Denmark (Oct. 2006).

[18] Collins, D., Zijdenbos, A., Kollokian, V., Sled, J., Kabani, N., Holmes, C., and Evans, A., "Design and Construction of a Realistic Digital Brain Phantom," *IEEE Trans. on Medical Imaging* **17**(3), 463–468 (1998). http://www.bic.mni.mcgill.ca/brainweb.

[19] Fornefett, M., Rohr, K., and Stiehl, H., "Radial Basis Functions with Compact Support for Elastic Registration of Medical Images," *Image and Vision Computing* **19**(1-2), 87–96 (2001).